Double-Sided Surface Passivation of 3D Perovskite Film for High-Efficiency Mixed Dimensional Perovskite Solar Cells

Md Arafat Mahmud, The Duong, Yanting Yin, Huyen T. Pham, Daniel Walter, Jun Peng, Yiliang Wu, Li Li, Heping Shen, Nandi Wu, Naeimeh Mozaffari, Gunther Andersson, Kylie R. Catchpole, Klaus J. Weber, and Thomas P. White**

Dr. M. A. Mahmud, Dr. T. Duong, Dr. D. Walter, Dr. J. Peng, Dr. Y. Wu, Dr. H. Shen, N. Wu, N. Mozaffari, Prof. K. R. Catchpole, Dr. K. J. Weber, Dr. T. P. White

Research School of Electrical, Energy and Materials Engineering, The Australian National University, Canberra, ACT 2601, Australia

E-mail: mdarafat.mahmud@anu.edu.au, thomas.white@anu.edu.au

Dr. Y. Yin, Prof. G. Andersson
Flinders Institute for Nanoscale Science and Technology, Flinders University, Adelaide SA 5042, Australia

Flinders Microscopy and Microanalysis, College of Science and Engineering, Flinders University, Adelaide, SA 5042, Australia

Huyen T. Pham

Department of Electronic Materials Engineering, Research School of Physics, The Australian National University, Canberra, ACT 2601, Australia

This is the author manuscript accepted for publication and has undergone full peer review but has not been through the copyediting, typesetting, pagination and proofreading process, which may lead to differences between this version and the Version of Record. Please cite this article as doi: 10.1002/adfm.201907962.

Dr Li Li

Australian National Fabrication Facility, Department of Electronic Materials Engineering, The Australian National University, Canberra, ACT 2601, Australia

Keywords: mixed dimensional perovskite, solar cells, passivation, surface bandgap widening

Defect-mediated carrier recombination at the interfaces between perovskite and neighboring charge transport layers limits the efficiency of most state-of-the-art perovskite solar cells. Passivation of interfacial defects is thus essential for attaining cell efficiencies close to the theoretical limit. In this work, we demonstrate a novel double-sided passivation of three-dimensional (3D) perovskite films with thin surface layers of bulky organic cation based halide compound forming two-dimensional (2D) layered perovskite. We report highly efficient (22.77%) mixed dimensional perovskite devices with a remarkable open-circuit voltage of 1.2 V for a bulk perovskite film having an optical bandgap of ~1.6 eV. Using a combination of experimental and numerical analysis, we show that the double-sided surface layers provide effective defect passivation at both the electron and hole transport layer interfaces, suppressing surface recombination on both sides of the active layer. Despite the semi-insulating nature of the passivation layers, we observe an increase in the fill factor of optimized cells. The efficient carrier extraction is explained by incomplete surface coverage of the 2D perovskite layer, allowing charge transport through localized unpassivated regions, similar to tunnel-oxide passivation layers used in silicon photovoltaics. The demonstration of effective double-side passivation with a single material expands the application of 2D layered perovskite materials in mixed-dimensional perovskite solar cells and provides new insights into their surface passivation mechanism. Optimization of the defect passivation and charge transport properties of these films has the potential to further increase cell efficiencies.

1. Introduction

Within a decade the power conversion efficiency (PCE) of perovskite solar cells (PSCs) has risen from 3.8% to over 25%.[1] This rapid development, coupled with the potential for low-cost fabrication compared to conventional crystalline silicon (c-Si) solar cells, continues to drive worldwide research into this emerging photovoltaic (PV) technology. In pursuit of even higher device performance, substantial research is being undertaken to improve the crystal quality of perovskite films as well as the charge extraction at the perovskite/electron transport layer (ETL) or perovskite/hole transport layer (HTL) interface.[2]

Commonly used solution-processed three-dimensional (3D) polycrystalline perovskite films exhibit notable structural defects/trap states, which lead to non-radiative carrier recombination, and a reduction in open circuit voltage well below the theoretical limit.[3] In addition, current-voltage hysteresis in PSCs is linked to the interaction of defects and mobile ions,[4] and may adversely affect the long-term stability of perovskite devices.[5] In PSCs, a major contributor to these trap-assisted carrier recombination phenomena are surface defects at the perovskite/electron transport layer (ETL) and perovskite/hole transport layer (HTL) interfaces, [6] indicating the importance of developing effective surface passivation techniques. A number of recent studies involving surface passivation have demonstrated suppressed non-radiative carrier recombination and consequently high open circuit voltage (V_{OC}) and enhanced PCE.[3a, 6-7] These surface passivation techniques include the incorporation of excess PbI_2 in the perovskite layer,[7d, 7j] controlled doping of perovskite,[7b, 7e, 8] ETL[7h, 7i] or HTL,[3d] insertion of a passivation layer at one or both of the perovskite/ETL[6c, 7c, 7f, 7g, 9] or perovskite/HTL[3a, 6a, 6b] interfaces.[6d]

Among the reported techniques, incorporation of large alkyl-ammonium cation based halide compounds has attracted substantial research interest recently due to their hydrophobic property and concomitant effect on device stability.[6b, 7e, 8, 10] These compounds are either incorporated into the bulk of the 3D perovskite[7e, 8] or applied as a surface passivation layer either at perovskite/HTL interface in normal (n-i-p) structured PSCs[3a, 6a, 6b, 7a, 11] or perovskite/ETL interface in inverted (p-i-n) structured PSCs.[7c, 7g, 9a] The 2D or 2D-layered perovskites formed with the incorporation of these halide compounds have been variously reported to contribute to the passivation of grain-boundaries of 3D perovskite;[8, 10b] enhancement in the crystallinity of the bulk perovskite;[6b, 8] favorable band alignment of perovskite film for cascaded charge transfer;[3a, 12] and the inactivation of interfacial trap-states.[6a, 6b] Since both perovskite/ETL and perovskite/HTL interfaces suffer from trap-assisted

carrier recombination,[13] application of 2D passivation layers on both interfaces of a cell is a natural extension of these previous works, but one that has not yet been reported in the literature. The rationale behind such double-sided 2D passivation also lies on the previous successful implementation of poly(methyl methacrylate) (PMMA) based dual-sided interface passivation[6d] and graphene/graphene oxide[14] in PSCs for enhanced PCE. However, the semi-insulating nature of 2D perovskites based on bulky organic cations [9a] requires a trade-off between having a sufficiently thick layer for effective surface passivation, while maintaining good carrier conductivity to allow efficient charge transport between the perovskite active layer and the transport layers.

Here, we demonstrate highly efficient (maximum PCE: 22.77%) mixed dimensional PSCs via double-sided passivation of 3D quadruple cation perovskite ($Cs_{0.07}Rb_{0.03}FA_{0.765}MA_{0.135}PbI_{2.55}Br_{0.45}$, MA: methyl ammonium, FA: formamidinium) films with n-butylammonium iodide ($C_4H_{12}IN$; n-BAI) in an n-i-p device configuration. The resulting symmetric passivating layer structure substantially reduces non-radiative recombination at both perovskite/charge transport layer interfaces. This is confirmed by enhanced V_{OC} and fill factor (FF) of passivated PSCs and is substantiated by steady-state photoluminescence intensity, photoluminescence (PL) imaging, time-resolved photoluminescence (TR-PL) characterization and X-ray diffraction (XRD) spectral peak analysis. The champion device with double-sided 2D passivation demonstrates a remarkable V_{OC} of 1.20V, and a stabilized PCE of 22.60% with negligible photo-current hysteresis. Using a combination of ultraviolet photoelectron spectroscopy (UPS)[15] surface analysis and numerical device simulations, we propose that discontinuous 2D perovskite layers chemically passivate defects on the surface of the 3D perovskite film, while simultaneously allowing efficient localized charge extraction via pinholes or similar unpassivated regions. This mechanism is similar to that exploited in tunnel-oxide passivating

contacts in crystalline silicon solar cells. The insights presented in this work open new opportunities for further enhancement of PCE with mixed dimensional 2D/3D PSCs.

2. Results and Discussion

To compare the effect of 2D interlayer passivation on device performance, PSCs with control (no passivation) as well as single-sided (SS) passivation (at perovskite/HTL interface) with six different concentrations of n-BAI (0.5 mg/ml, 1 mg/ml, 2 mg/ml, 3 mg/ml, 4 mg/ml and 5 mg/ml in 2-propanol) were prepared. Keeping the other fabrication steps identical, 20 cells of each kind were fabricated. The overall device structure with SS passivation was FTO/compact TiO_2 (cp-TiO_2)/mesoporous TiO_2 (mp-TiO_2)/PMMA:PCBM[7f]/$Cs_{0.07}Rb_{0.03}FA_{0.765}MA_{0.135}PbI_{2.55}Br_{0.45}$ perovskite/n-BAI passivation layer/Spiro-OMeTAD/Au. For double-sided passivation, an additional n-BAI layer was incorporated between PMMA:PCBM and perovskite layers (Figure 1a), more details of which are discussed below. Individual layer thicknesses are shown in the cross-section scanning electron microscopy (SEM) image of a representative PSC (Figure 1b). No distinct 2D surface layer could be clearly identified at the interface between 3D perovskite and Spiro-OMeTAD HTL from cross-sectional SEM images; hence high-resolution transmission electron microscopy (HRTEM) cross-section imaging was conducted (Figure 2). As demonstrated in Figures 2a-2b and Figure S1, we observe a thin, non-uniform and discontinuous interlayer at the 3D perovskite/HTL interface. To confirm that this thin layer is the 2D perovskite we measured the interplanar spacing at representative locations close to the interface as shown in Figure 2d. The 3D perovskite layer is identified by the characteristic interplanar spacing of 3.52 Å, which is clearly different from the interplanar spacing of 9.1 Å exhibited by 2D surface layer. Based on this we estimate the maximum

layer thickness of the 2D perovskite to be approximately 20 nm (Figure 2c). Nevertheless, as the HRTEM images reveal, the 2D surface layer is non-uniform and discontinuous at the 3D perovskite/HTL interface, which has substantial implications on the device performance as discussed in the following sections.

The statistical chart-boxes presented in Figures 1c-1f show the distribution of photovoltaic performance and current-voltage (J-V) parameters of the fabricated devices. As observed from Figures 1c-1f, passivated (single-sided) cells demonstrate higher photovoltaic performance compared to the control PSCs. The performance enhancement mostly originates from increased V_{OC} and FF, consistent with interface passivation from the n-BAI. The average V_{OC} value monotonically increases with increasing n-BAI concentration, whereas the average short-circuit current density (J_{SC}) and FF start to drop with concentrations over 1 mg/ml. The reduction in J_{SC} and FF for higher n-BAI concentrations can be attributed to the increased 2D film thickness and concomitant reduction in film conductivity (discussed in more detail below).[6b] The optimum n-BAI concentration for the single-sided passivation was found to be 1 mg/ml. This value was chosen to develop PSCs with double-sided (DS) passivation.

Figure 3a shows the J-V curves of the champion control and double-side passivated PSCs at a scan rate of 50 mV/s. The control PSC demonstrates moderate hysteresis, yielding an efficiency of 20.02% (19.65%) with V_{OC} = 1.16 V (1.15 V), J_{SC} = 23.80 mA/cm^2 (23.79 mA/cm^2) and FF = 72.55% (71.87%), from reverse (forward) J-V scan. In contrast, the champion DS PSC has an efficiency of 22.77% from reverse scan (22.59% from forward scan) with V_{OC} = 1.20V (1.20 V), J_{SC} = 23.94 mA/cm^2 (23.97 mA/cm^2) and FF = 79.31% (78.56%). The DS PSC also exhibits a higher steady state PCE (~22.60%) at maximum power point voltage (V_{MPP}=1.008V) compared to that (19.88%, V_{MPP} = 0.957V) of the control device (Figure 3b). It is also notable that the MPP stabilization occurs more rapidly for the

passivated cells compared to the control, and the current-voltage hysteresis is also reduced, as indicated by the hysteresis indices calculated at different scan rates (Figure 3c). These improvements in cell performance are clear indications of enhanced interface passivation provided by the n-BAI based interlayer (we discuss this further in relation to numerical device simulations below). External quantum efficiency (EQE) measurements were conducted on both PSCs (Figure S2) and as expected, there was no significant difference in the integrated J_{SC} values of the control and DS PSCs.

To get a more complete understanding of the performance enhancement in single and double-side passivated cells, we next investigate the structural, optical and electrical performance of passivated and unpassivated cells and films. First, XRD measurements of the relevant films were taken to investigate possible structural changes at the surface, or in the underlying 3D perovskite film (Figure S3a). As expected, both control and passivated films exhibit characteristic XRD diffraction peaks for 3D perovskite, however, we also observe prominent 2D perovskite peaks for the films having n-BAI concentration over 3 mg/ml. Film crystallinity is also somewhat enhanced in passivated samples, with the narrowest peak width (full width at half maximum, FWHM) of the major 3D perovskite peak (110) occurring for an n-BAI concentration of 1 mg/ml (Figure S3b). This is also reflected by the lowest microstrain and dislocation density calculated for 1 mg/ml perovskite film from XRD spectral peak fitting analysis (Figure S3c). Enhanced crystallinity and lower surface strain with 1 mg/ml n-BAI concentration may contribute to the enhanced FF of the corresponding PSCs. The absence of an observable 2D perovskite peak for the optimum n-BAI concentration of 1 mg/ml may also support previous reports[10,11] suggesting that the formation of the 2D perovskite phase is not essential for enhanced device performance; rather that the unconverted halide layer itself may provide effective surface passivation, reduce surface strain and enhance 3D perovskite crystallinity.

To verify the presence of n-BAI components on the perovskite surface at low concentration (1 mg/ml), we have conducted surface elemental analysis of control and passivated films with X-ray photoelectron spectroscopy (XPS). From the deconvolution of high resolution C 1s XPS spectra (Figure S4a), we find that the weighting factor for the C-C bond on the surface increases proportionally with the n-BAI concentration (Figure S4b). This can be directly attributed to the presence of the long carbon chain of n-BAI at the surface, confirming the chemical modification of the perovskite surface, even at very low n-BAI concentrations.

Along with the surface chemistry, the addition of the n-BAI layer also induces minor changes to the surface morphology of the 3D perovskite films, as evidenced from the top-view SEM images of the films presented in Figure S5. Perovskite grain size initially increases slightly with increasing n-BAI concentration; however gradual reduction in grain size is observed for concentrations over 1 mg/ml. This trend in the variation of perovskite grain size with n-BAI concentration is consistent with the values of crystallite dimension calculated from XRD spectral analysis using the Scherrer equation (Figure S3b)[16] and has also been observed in previous literature on mixed 2D/3D PSC.[6b] Although large perovskite grain-size has been linked to enhanced V_{OC} of PSCs in some literature,[17] we do not observe a direct link between the perovskite grain size and the V_{OC} values of the fabricated PSCs. Device V_{OC} monotonically increases up to an n-BAI concentration of 5 mg/ml, whereas the variation in perovskite grain size does not follow any proportional relationship. We also do not observe a significant change in surface roughness between the control and optimum passivated perovskite films from atomic force microscopy (AFM) characterization (Figure S6), which suggests that the modification in surface morphology or topology with the passivating layer does not play a major role in the performance enhancement of the mixed dimensional PSCs.

We also conducted optical characterization of the perovskite films using ultraviolet-visible-near infrared (UV-Vis-NIR) spectroscopy. Absorbance and transmittance spectra of perovskite films on FTO substrates are presented in Figure S7a and Figure S7b, respectively. The absorbance of the passivated perovskite films slightly reduces with the increase in n-BAI concentration at the far end of the visible spectrum (~660 nm-750 nm), which is also observed in the respective transmittance profiles in the same wavelength region. The reduced absorption with higher n-BAI concentration at longer wavelength can be attributed to the partial conversion of 3D perovskite into 2D at the surface.[3a, 7e] However, the slight reduction in film absorbance has a negligible effect on the short-circuit current of complete cells. The optical bandgaps of the control and passivated perovskite films were also checked with a Tauc plot and no significant variation was found (Figure S7c).

Subsequently, we measured the steady-state PL spectra of control and n-BAI modified films on ETL-coated FTO substrates to investigate carrier recombination before and after passivation (Figure 4a). The peak PL intensity increases with increasing n-BAI concentration, consistent with the observed trend in device V_{OC}. This confirms the suppression of non-radiative carrier recombination.[6a, 6b] Here, it is worth mentioning that the PL intensity with 1 mg/ml DS perovskite is higher than the single-sided 1 mg/ml perovskite film, corroborating the beneficial role of the double-sided surface passivation in mitigating trap-states at both interfaces of the 3D perovskite film and its neighboring charge transport layers. Interestingly, we do not observe any PL emission associated with the higher-bandgap 2D perovskite material, as has been noted in similar works with other large-cation treatments.[3a, 10b]

We can directly observe a reduction in non-radiative recombination by PL imaging of control, SS and DS passivated cells under open-circuit conditions (Figures 4b-4d). As expected, both the passivated cells (SS and DS) exhibit higher PL intensity compared to the control cell. Under steady-state open

circuit conditions, the suppressed non-radiative recombination phenomena contribute to excess carrier density in the photoactive perovskite layer, resulting in enhanced V_{OC} through increased quasi Fermi level splitting.[18] Thus, the passivated cells exhibit higher V_{OC} compared to the control device. The DS PSC also demonstrates higher PL intensity compared to SS PSC, consistent with the higher V_{OC} compared to 1 mg/ml SS PSCs. The PL intensity keeps increasing with halide concentration up to 5 mg/ml (Figure S8), following the observed V_{OC} trend in Figure 1d. As expected, these observed increases in steady-state PL emission intensity are well correlated with increased transient lifetimes observed from time-resolved-photoluminescence (TRPL) measurements. Details of TRPL measurements on passivated and unpassivated films with several different layer combinations are provided in the supporting information (see Figures S9-S10 and relevant text).

The experimental results presented so far are entirely consistent with chemical passivation of interfacial defects, whereby the interface defect density on the surface of the 3D perovskite active layer is reduced by the n-BAI treatment. An alternative explanation, proposed in several prior studies of mixed dimensional PSCs,[3a, 12] is improved energy band alignment between the perovskite and transport layer(s), resulting in electronic passivation and more efficient carrier extraction. In the following analysis we combine experimental energy level data from UPS and inverse photoemission spectroscopy (IPES) measurements with numerical device simulations to clarify the role of the 2D passivation layers. While we cannot rule out an electronic contribution, our analysis provides strong support for chemical passivation being the dominant enhancement mechanism in our cells.

Figure 5a shows the evolution of the secondary electron edge from the UPS curves for perovskite films (on FTO substrates) and Figure 5b shows the valence band (VB) region of the respective spectra. The estimated workfunction values for the control, 1 mg/ml, 3 mg/ml and 5 mg/ml perovskite films are 3.4±0.1 eV, 2.9±0.1 eV, 3.3±0.1 eV and 3.3±0.1 eV, respectively. The values of

VBM of the control and passivated perovskite films are presented in Figure 5d, extracted from the linear extrapolation of the leading edges of the magnified UPS curves in the VB region (Figure 5c). All passivated films show a slight upshift in VBM compared to the control perovskite film. Since the HTL is constant for all the PSCs, the upshifted VBM in passivated perovskite films reduces the VBM/HOMO (highest occupied molecular orbital) energy gap between perovskite and HTL, compared to control. Similar valence band shifts have been reported for other 2D passivation layers[3a] and may contribute to enhanced hole extraction in the passivated devices. On the other hand, considering the perovskite/ETL interface, since the ETL is identical for all devices, the elevated VBM associated with the passivation layer increases the VB energy gap at the interface with the ETL, potentially contributing to improved hole blocking[19] compared to reference devices.

Although the observed shifts in VBM suggest the possibility of electronic passivation and improved carrier extraction, we must also consider the effect of changes to the conduction band alignment at the same interfaces. The conduction band minima (CBM) of the control and passivated perovskite films are also shown in Figure 5d. It is apparent that the shift in CBM energy with the addition of the thin n-BAI layer is larger than the VBM shift, consistent with the surface bandgap widening identified in previous reports on mixed-dimensional PSC.[3a] This increase in the CBM would introduce an energy barrier for electrons to transfer to the ETL. Thus, while the upshift in the VBM is predicted to have a positive impact on hole extraction and hole blocking properties at the HTL and ETL interfaces respectively, the corresponding increase in CBM energy should have a negative impact on electron extraction at the ETL interface. This is inconsistent with the experimental observation that the n-BAI treatment can be applied to both sides of the cell, resulting in significant improvement in Voc and FF in each case. To resolve this apparent contradiction, we propose that the dominant contribution of the 2D interfacial layer is chemical passivation of surface defects, rather than electronic passivation,

while efficient carrier extraction is maintained by incomplete surface coverage of the ultrathin passivation layer. Experimental and numerical evidence supporting this interpretation are discussed below.

Singular-value decomposition (SVD) analysis of the UPS spectra indicates that the valence electron spectra of the passivated films in Figure 5 include contributions from both 2D and 3D perovskite (see Figures S11-S12 and relevant text in supplementary section). Given that the sampling depth of the UPS measurements is on the order of 3 nm, this observation suggests three possible interpretations: (a) the 2D passivation layer is continuous, but <3nm thick so there is a contribution from the underlying 3D perovskite film; (b) the passivation layer is discontinuous, leaving some exposed 3D material at the surface; (c) the surface layer consists of a mixture of 2D and 3D materials formed during the spin-coating of the n-BAI on the 3D film surface. Interpretation (a) is unlikely given that such thin layers processed by solution are rarely continuous or pinhole-free, leaving us to conclude that alternatives (b) or (c) are most likely. This provides a plausible explanation for why the 2D passivation layer can be applied effectively at both the ETL and HTL interfaces. In regions where the 2D layer forms on the surface of the 3D film, it passivates defects, but also increases the local series resistance; meanwhile, the remaining areas of exposed 3D perovskite contact directly with the transport layer, providing efficient carrier extraction, albeit with a higher defect density. The proposed charge transfer mechanism through the semi-insulating 2D layer is thus similar to the tunnel-oxide passivation layers used in silicon photovoltaics,[20] which has been discussed later.

To explore this hypothesis further, we next use numerical device models developed in-house [21] to test whether the observed increase in voltage and fill factor, and reduction in hysteresis, is consistent with defect passivation at the perovskite/transport layer interfaces. We performed transient simulations of a prototypical perovskite solar cell (i.e. TiO_2-$MAPbI_3$-Spiro) in which two

ionic species of opposite polarity are mobile. Interface recombination was modelled using simplified Shockley-Read Hall (SRH) statistics in which charge carriers on both sides of the interface are free to interact through interface traps. We simulated the influence of surface recombination velocities (SRVs) for both holes and electrons by adjusting their level uniformly at each interface. Thus, we assume that the passivation is equally effective at both interfaces. We simulated the current density-voltage (J-V) curves using a time-varying voltage equivalent to the 50 mV/s scan rate of the experimental J-V measurement protocol. Secondly, we simulated the transient response of the photocurrent to an abrupt application of forward bias at the maximum power-point voltage and one-sun equivalent illumination. Note that we have not attempted to match the absolute magnitude of the cell characteristics (eg: V_{oc} and J_{sc}) precisely as the aim of the simulations is to explore the consistency between changing interface recombination and experimental performance of the cell. Nevertheless, the relative trends in performance characteristics can be compared to the experimental results.

As interface recombination increases, the simulated transient J-V curves exhibit a decrease in both open-circuit voltage and fill-factor and a relatively nominal change in short-circuit current (Figure 6a) consistent with the experimental data. Voltage and fill-factor loss are ultimately attributable to charge carrier recombination at the interfaces. At short-circuit, however, charge extraction is still near 100% for moderate surface recombination velocities since diffusion lengths exceed the thickness of the perovskite absorber. The first indications of J_{sc} reduction are seen at SRV = 1000 cm/s in Figure 6c. Our simulations also suggest an important influence of the mobile ions' mobility in reproducing the relatively large decline in fill-factor with increasing SRV. A detailed explanation is beyond the scope of this work, but we provide here a brief overview. At the initial, stabilised, open-circuit voltage conditions prior to the J-V sweep, the mobile ions accumulate on the perovskite side

of the transport layer interfaces in response to the built-in electric field in the perovskite absorber (we assume that the ions are blocked by the transport layers). The electric field generated by the net ionic charge at the interface repels minority carriers from the interface and any recombination-active defects there. At each interface, the high density of majority carriers in the respective transport layer provide an effectively infinite source for recombination, resulting in a recombination bottleneck imposed by the availability of comparatively rare minority carriers. As the terminal voltage moves towards short-circuit, the built-in electric field reduces and the net ionic charge at the interfaces decreases. This in turn reduces the electric field strength at the interface that is working against minority carrier transport. Therefore, the voltage sweep toward short-circuit results in a proportionally larger loss of photocurrent due to ion movement and thus a reduction in fill-factor. The magnitude of this effect depends on the rate of change of the terminal voltage relative to the mobility of the ionic defects. This is fundamentally the same mechanism invoked to describe the voltage sweep rate-dependence of the hysteresis index of PSCs[4b] except that here we emphasize that the apparent fill-factor decrease as a result of interface recombination depends upon the choice of sweep rate and ion mobility in our simulations. Although the sweep rate is fixed by the experimental conditions (at 50 mV/s), we are ultimately uncertain about the mobilities of the mobile ions in this perovskite composition. As a result, we have not attempted an exact fit to our experimental results, but we note that the ion parameters are plausible within published values of other perovskite compositions (See Tables S4-S5 and relevant text in Supplementary section). We instead emphasize that the movement of ions during the J-V sweep is likely a necessary factor in the significant fill factor increase seen between the control cell and the 1 mg/ml n-BAI concentration.

Next, we consider the experimental transient response of the maximum power-point current which stabilized significantly faster in cells passivated with the n-BAI layers (Figure 3b). Our simulations

demonstrate that this is also consistent with reduced interface recombination (Figure 6b). Hysteretic phenomena in PSCs result from Coulombic coupling between ions and electrons (and holes) and subsequent modification of recombination currents. The manifestation of hysteresis requires both mobile ions and non-radiative recombination mechanisms [21b, 22]. Accordingly, reducing interface recombination in our simulations— in addition to increasing the magnitude of the maximum power-point current— increases the rate at which the photocurrent reaches steady state. This is despite each simulation predicting similar redistribution of ions through the perovskite absorber as a result of a step to forward bias.

Our simulations therefore show that changes in the transient electrical characteristics of the 1 mg/ml n-BAI PSCs relative to the control case are consistent with reduced interface recombination in the presence of mobiles ions. It is notable that the 1 mg/ml n-BAI layer can achieve this with minimal influence on series resistance and fill-factor. This is an improvement over existing voltage-enhancing passivation methods such as PMMA:PCBM,[7f] which also reduce fill-factor, suggesting a resistive bottleneck to charge extraction. In this work, the 1 mg/ml n-BAI layer does not reduce fill-factor. This is despite the change in the electron affinity shown in Figure 5d that predicts an energy barrier to electron extraction of approximately 0.7 V at the ETL (Figure S13). Although our simulations do not address directly why the n-BAI film does not increase resistance, we can posit theories based on analogous technologies employed in other photovoltaic devices, and supported by the UPS data discussed previously.

We know from the cross-section HRTEM image of the device (Figure S1) that the n-BAI film is non-uniform and discontinuous along the 3D perovskite/HTL interface and the thickness can be well below its maximum thickness (20 nm) in places. This suggests a similarity with tunnel-oxide passivation layers in silicon photovoltaics, in which an ultrathin (≤ ~15 Å) silicon dioxide layer is

grown on a silicon substrate prior to the deposition of charge-selective transport layers or metal contacts.[23] A notable example is the tunnel oxide passivated contact (TOPCon) technology, which has achieved silicon solar cell efficiencies in excess of 25%.[20] Relevant to the results here, the contact resistance of the tunnel oxide structure increases dramatically (tunnelling probability decreases) for oxide thicknesses greater than ~15 Å, with an extremely high sensitivity to film thickness (e.g. FF declines by 70% absolute as the silicon oxide layer increases from 15 to 20 Å[23b]). It may be that the decline in cell performance for n-BAI concentrations above 1 mg/ml, which is dominated by a reduced fill factor, is the result of nanometer-scale increases in thickness which are below our ability to discern through electron microscopy but are nonetheless influential on the efficiency of the tunnelling process.

However, lower fill factor for higher n-BAI concentrations is also correlated with improved voltages, which may suggest that the lower concentration n-BAI layers are not continuous, containing gaps or pinholes through which low resistance contact is made to the transport layers at the expense of increased interface recombination. This is consistent with the SVD analysis of the UPS spectra of the passivated perovskite films discussed above. Continuing our analogy to tunnelling silicon oxides, it is known that process conditions (including annealing temperatures) can affect pinhole density in ultra-thin oxide layers. In fact, process conditions have been deliberately manipulated to introduce pinholes in thicker layers (> 20 Å) in order to facilitate charge transport, albeit by reducing passivation quality.[24] The continued increase in open-circuit voltage with higher concentrations even as fill-factor declines, could be explained by increased n-BAI coverage if the film were too thick to allow effective electron conduction via tunnelling.

If the high performance of the 1 mg/mL n-BAI cells relies on the passivation layer being discontinuous at the interface, as our analysis indicates, future optimisation of the coverage fraction

to maximise the voltage/fill-factor trade-off may provide further efficiency gains. Temperature-dependent current-voltage measurements have been used to separate tunnelling vs pinhole transport mechanisms in silicon-dioxide test structures,[25] suggesting an avenue for future investigation of charge transport mechanisms through ultra-thin passivating layers in PSCs.

Following reports of improved stability in cells passivated with 2D perovskite films,[6b, 7e, 8, 10] we investigated the light stability of un-encapsulated PSCs under continuous light soaking in a N_2 atmosphere (1 sun) while holding the devices at their maximum power point. After 20 hours of light soaking, both the control and passivated cells showed a relative efficiency decrease of approximately 10%. Thus, the efficiency-optimized 2D passivation layer does not appear to have a significant impact (positive or negative) on the device stability under steady state illumination (Figure S14). This may be a consequence of the incomplete surface coverage in cells optimized for efficiency as discussed above, or it may indicate that other degradation mechanisms are dominant in these cells, for example those associated with the hygroscopic Spiro-OMeTAD layer, which is known to contribute to cell instability. Replacing the Spiro-OMeTAD with dopant-free novel HTLs[7a, 26] is therefore a priority for improving long term cell stability of PSCs, but this is beyond the scope of the current study.

3. Conclusion

In summary, we have demonstrated the first successful implementation of double-side passivation of 3D perovskite films with a bulky organic cation based n-BAI compound, resulting in a mixed-dimensional PSC with a 22.60% stabilized PCE. The optimized n-BAI surface modification (from 1 mg/ml n-BAI precursor) provides outstanding passivation at both interfaces between perovskite and

neighboring charge transport layers, contributing to a remarkable V_{OC} of 1.2 V, which is one of the highest open-circuit voltages reported for perovskite cells with an optical bandgap of ~1.6 eV. In contrast to previous reports that have emphasized improved energy level alignment when discussing the performance enhancement offered by 2D perovskite interlayers,[3a, 12] our results indicate that chemical passivation of interfacial defects plays a dominant role. The ultrathin n-BAI based layers effectively passivate surface defects, reducing the surface recombination velocity and suppressing interfacial carrier recombination at both the perovskite/HTL and perovskite/ETL interfaces. Efficient carrier extraction is maintained by ensuring that the passivation layer is discontinuous, providing conductive pathways between the 3D perovskite and the transport layers. This trade-off between passivation quality and charge extraction enables both enhanced V_{OC} and FF in double-sided passivated devices, compared to unpassivated or single-side passivated PSCs. Further improvement in device performance may be possible by optimizing the surface coverage of the passivation layer, by tailoring the crystal orientation of the 2D interlayer for enhanced charge collection[27] and by exploring the synergistic effect of mixed halide compounds to achieve both energy band alignment and chemical passivation properties.

4. Experimental Section

Experimental details are provided in the Supporting Information section.

Supporting Information

Supporting Information is available from the Wiley Online Library or from the author.

Acknowledgements

The work was supported by the Australian Government through the Australian Renewable Energy Agency (ARENA) and the Australian Research Council (ARC). T.P.W is the recipient of an Australian Research Council Australian Future Fellowship (project number FT180100302) funded by the Australian Government. Responsibility for the views, information or advice herein is not accepted by the Australian Government. This work has been made possible through the access to the ACT Node of the Australian National Fabrication Facility (ANFF @ ANU).

Conflict of Interest

The authors declare no conflict of interest.

Received: ((will be filled in by the editorial staff))
Revised: ((will be filled in by the editorial staff))
Published online: ((will be filled in by the editorial staff))

References

[1] National Renewable Energy Laboratory (NREL) Efficiency Chart, https://www.nrel.gov/pv/cell-efficiency.html, accessed: 12 June, 2019.

[2] a) E. Aydin, M. De Bastiani, S. De Wolf, *Advanced Materials* **2019**, 31, 1900428; b) S. I. Seok, M. Grätzel, N.-G. Park, *Small* **2018**, *14*, 1704177.

[3] a) S. Gharibzadeh, B. Abdollahi Nejand, M. Jakoby, T. Abzieher, D. Hauschild, S. Moghadamzadeh, J. A. Schwenzer, P. Brenner, R. Schmager, A. A. Haghighirad, L. Weinhardt, U. Lemmer, B. S. Richards, I. A. Howard, U. W. Paetzold, *Adv. Energy Mater.* **2019**, *9*, 1803699; b) P. Schulz, *ACS Energy Lett.* **2018**, *3*, 1287; c) M. Stolterfoht, C. M. Wolff, J. A. Márquez, S. Zhang, C. J. Hages, D. Rothhardt, S. Albrecht, P. L. Burn, P. Meredith, T. Unold, D. Neher, *Nat. Energy* **2018**, *3*, 847; d) J.-P. Correa-Baena, W. Tress, K. Domanski, E. H. Anaraki, S.-H. Turren-Cruz, B. Roose, P. P.

Boix, M. Grätzel, M. Saliba, A. Abate, A. Hagfeldt, *Energy Environ. Sci.* **2017**, *10*, 1207; e) W. S. Yang, B.-W. Park, E. H. Jung, N. J. Jeon, Y. C. Kim, D. U. Lee, S. S. Shin, J. Seo, E. K. Kim, J. H. Noh, S. I. Seok, *Science* **2017**, *356*, 1376; f) S. D. Stranks, *ACS Energy Lett.* **2017**, *2*, 1515; g) W. Tress, *Adv. Energy Mater.* **2017**, *7*, 1602358.

[4] a) B. Chen, M. Yang, S. Priya, K. Zhu, *J. Phys. Chem. Lett.* **2016**, *7*, 905; b) W. Tress, N. Marinova, T. Moehl, S. M. Zakeeruddin, M. K. Nazeeruddin, M. Grätzel, *Energy Environ. Sci.* **2015**, *8,* 995.

[5] F. Huang, L. Jiang, A. R. Pascoe, Y. Yan, U. Bach, L. Spiccia, Y.-B. Cheng, *Nano Energy* **2016**, *27*, 509.

[6] a) Q. Jiang, Y. Zhao, X. Zhang, X. Yang, Y. Chen, Z. Chu, Q. Ye, X. Li, Z. Yin, J. You, *Nat. Photonics* **2019**, DOI: 10.1038/s41566-019-0398-2; b) Y. Cho, A. M. Soufiani, J. S. Yun, J. Kim, D. S. Lee, J. Seidel, X. Deng, M. A. Green, S. Huang, A. W. Y. Ho-Baillie, *Adv. Energy Mater.* **2018**, *8*, 1703392; c) X. Zheng, B. Chen, J. Dai, Y. Fang, Y. Bai, Y. Lin, H. Wei, Xiao C. Zeng, J. Huang, *Nat. Energy* **2017**, *2*, 17102; d) J. Peng, J. I. Khan, W. Liu, E. Ugur, T. Duong, Y. Wu, H. Shen, K. Wang, H. Dang, E. Aydin, X. Yang, Y. Wan, K. J. Weber, K. R. Catchpole, F. Laquai, S. De Wolf, T. P. White, *Adv. Energy Mater.* **2018**, *8*, 1801208.

[7] a) E. H. Jung, N. J. Jeon, E. Y. Park, C. S. Moon, T. J. Shin, T.-Y. Yang, J. H. Noh, J. Seo, *Nature* **2019**, *567*, 511; b) M. Abdi-Jalebi, Z. Andaji-Garmaroudi, S. Cacovich, C. Stavrakas, B. Philippe, J. M. Richter, M. Alsari, E. P. Booker, E. M. Hutter, A. J. Pearson, S. Lilliu, T. J. Savenije, H. Rensmo, G. Divitini, C. Ducati, R. H. Friend, S. D. Stranks, *Nature* **2018**, *555*, 497; c) T. Ye, A. Bruno, G. Han, T. M. Koh, J. Li, N. F. Jamaludin, C. Soci, S. G. Mhaisalkar, W. L. Leong, *Adv. Funct. Mater.* **2018**, *28*, 1801654; d) Q. Jiang, Z. Chu, P. Wang, X. Yang, H. Liu, Y. Wang, Z. Yin, J. Wu, X. Zhang, J. You, *Adv.*

Mater. **2017**, *29*, 1703852; e) Z. Wang, Q. Lin, F. P. Chmiel, N. Sakai, L. M. Herz, H. J. Snaith, *Nat. Energy* **2017**, *2*, 17135; f) J. Peng, Y. Wu, W. Ye, D. A. Jacobs, H. Shen, X. Fu, Y. Wan, T. Duong, N. Wu, C. Barugkin, H. T. Nguyen, D. Zhong, J. Li, T. Lu, Y. Liu, M. N. Lockrey, K. J. Weber, K. R. Catchpole, T. P. White, *Energy Environ. Sci.* **2017**, *10*, 1792; g) Y. Bai, S. Xiao, C. Hu, T. Zhang, X. Meng, H. Lin, Y. Yang, S. Yang, *Adv. Energy Mater.* **2017**, *7*, 1701038; h) F. Giordano, A. Abate, J. P. Correa Baena, M. Saliba, T. Matsui, S. H. Im, S. M. Zakeeruddin, M. K. Nazeeruddin, A. Hagfeldt, M. Graetzel, *Nat. Commun.* **2016**, *7*, 10379; i) M. Saliba, T. Matsui, K. Domanski, J.-Y. Seo, A. Ummadisingu, S. M. Zakeeruddin, J.-P. Correa-Baena, W. R. Tress, A. Abate, A. Hagfeldt, M. Grätzel, *Science* **2016**, *354*, 206; j) Q. Chen, H. Zhou, T.-B. Song, S. Luo, Z. Hong, H.-S. Duan, L. Dou, Y. Liu, Y. Yang, *Nano Lett.* **2014**, *14*, 4158.

[8] J.-W. Lee, Z. Dai, T.-H. Han, C. Choi, S.-Y. Chang, S.-J. Lee, N. De Marco, H. Zhao, P. Sun, Y. Huang, Y. Yang, *Nat. Commun.* **2018**, *9*, 3021.

[9] a) T. Zhao, C.-C. Chueh, Q. Chen, A. Rajagopal, A. K. Y. Jen, *ACS Energy Lett.* **2016**, *1*, 757; b) A. Abate, M. Saliba, D. J. Hollman, S. D. Stranks, K. Wojciechowski, R. Avolio, G. Grancini, A. Petrozza, H. J. Snaith, *Nano Lett.* **2014**, *14*, 3247.

[10] a) G. Grancini, C. Roldán-Carmona, I. Zimmermann, E. Mosconi, X. Lee, D. Martineau, S. Narbey, F. Oswald, F. De Angelis, M. Graetzel, M. K. Nazeeruddin, *Nat. Commun.* **2017**, *8*, 15684; b) D. S. Lee, J. S. Yun, J. Kim, A. M. Soufiani, S. Chen, Y. Cho, X. Deng, J. Seidel, S. Lim, S. Huang, A. W. Y. Ho-Baillie, *ACS Energy Lett.* **2018**, *3*, 647.

[11] T. Niu, J. Lu, X. Jia, Z. Xu, M.-C. Tang, D. Barrit, N. Yuan, J. Ding, X. Zhang, Y. Fan, T. Luo, Y. Zhang, D.-M. Smilgies, Z. Liu, A. Amassian, S. Jin, K. Zhao, S. Liu, *Nano Lett.* **2019**, DOI: 10.1021/acs.nanolett.9b02781.

[12] J. Lu, L. Jiang, W. Li, F. Li, N. K. Pai, A. D. Scully, C.-M. Tsai, U. Bach, A. N. Simonov, Y.-B. Cheng, L. Spiccia, *Adv. Energy Mater.* **2017**, *7*, 1700444.

[13] J. Kim, A. Ho-Baillie, S. Huang, *Sol. RRL* **2019**, *3*, 1800302.

[14] A. Agresti, S. Pescetelli, B. Taheri, A. E. Del Rio Castillo, L. Cinà, F. Bonaccorso, A. Di Carlo, *ChemSusChem* **2016**, 9, 2609.

[15] a) B. Andrea, L. Yan-Chun, M. Harald, *Surf. Sci.* **2008**, *602*, 3737; b) A. Berlich, Y. C. Liu, H. Morgner, *Radiat. Phys. Chem.* **2005**, *74*, 201.

[16] U. Holzwarth, N. Gibson, *Nat. Nanotechnol.* **2011**, *6*, 534.

[17] a) J. Chen, T. Shi, X. Li, B. Zhou, H. Cao, Y. Wang, *Appl. Phys. Lett* **2016**, *108,* 053302; b) C. Bi, Q. Wang, Y. Shao, Y. Yuan, Z. Xiao, J. Huang, *Nat. Commun.* **2015**, *6*, 7747.

[18] M. I. Dar, M. Franckevičius, N. Arora, K. Redeckas, M. Vengris, V. Gulbinas, S. M. Zakeeruddin, M. Grätzel, *Chem. Phys. Lett* **2017**, *683*, 211.

[19] X. Ma, P. Tang, D. Liu, J. Zhang, L. Feng, L. Wu, *ChemPhysChem* **2017**, 18, 2939.

[20] A. Richter, J. Benick, F. Feldmann, A. Fell, M. Hermle, S. W. Glunz, *Sol. Energy Mater. Sol. Cells* **2017**, *173*, 96.

[21] a) H. Shen, D. A. Jacobs, Y. Wu, T. Duong, J. Peng, X. Wen, X. Fu, S. K. Karuturi, T. P. White, K. Weber, K. R. Catchpole, *J. Phys. Chem. Lett.* **2017**, *8*, 2672; b) D. Walter, A. Fell, Y. Wu, T. Duong, C. Barugkin, N. Wu, T. White, K. Weber, *The J. Phys. Chem. C* **2018**, *122*, 11270.

[22] a) D. A. Jacobs, H. Shen, F. Pfeffer, J. Peng, T. P. White, F. J. Beck, K. R. Catchpole, *J. Appl. Phys* **2018**, *124*, 225702; b) P. Calado, A. M. Telford, D. Bryant, X. Li, J. Nelson, B. C. O'Regan, P. R. F.

Barnes, *Nat. Commun.* **2016**, *7*, 13831; c) S. van Reenen, M. Kemerink, H. J. Snaith, *J. Phys. Chem. Lett.* **2015**, *6*, 3808.

[23] a) F. Feldmann, M. Bivour, C. Reichel, M. Hermle, S. W. Glunz, *Sol. Energy Mater. Sol. Cells* **2014**, *120*, 270; b) J. Shewchun, R. Singh, M. A. Green, *J. Appl. Phys.* **1977**, 48, 765; c) M. B. F. Feldmann, C. Reichel, M. Hermle, S.W. Glunz, presented at 28th European Photovoltaic Solar Energy Conference and Exhibition **2013**.

[24] J. Y. Gan, R. M. Swanson, presented at IEEE Conference on Photovoltaic Specialists, 21-25 May 1990, **1990**.

[25] F. Feldmann, G. Nogay, P. Löper, D. L. Young, B. G. Lee, P. Stradins, M. Hermle, S. W. Glunz, *Sol. Energy Mater. Sol. Cells* **2018**, *178*, 15.

[26] K. Rakstys, S. Paek, P. Gao, P. Gratia, T. Marszalek, G. Grancini, K. T. Cho, K. Genevicius, V. Jankauskas, W. Pisula, M. K. Nazeeruddin, *J. Mater. Chem. A* **2017**, *5*, 7811.

[27] X. Zhang, G. Wu, W. Fu, M. Qin, W. Yang, J. Yan, Z. Zhang, X. Lu, H. Chen, *Adv. Energy Mater.* **2018**, 8, 1702498.

Figure 1. a. Schematic illustrating the layer sequence of a double-side passivated perovskite solar cell, b. Cross-section SEM image of the device demonstrating the thickness of the individual layer, Statistical box plots showing the variation in photovoltaic parameters for the control and passivated cells: c. Variation in PCE, d. Variation in V_{OC}, e. Variation in FF and f. Variation in J_{SC}. The data for the statistical distribution were taken from 20 cells of each kind and obtained from reverse scan at a scan rate of 50 mV/s

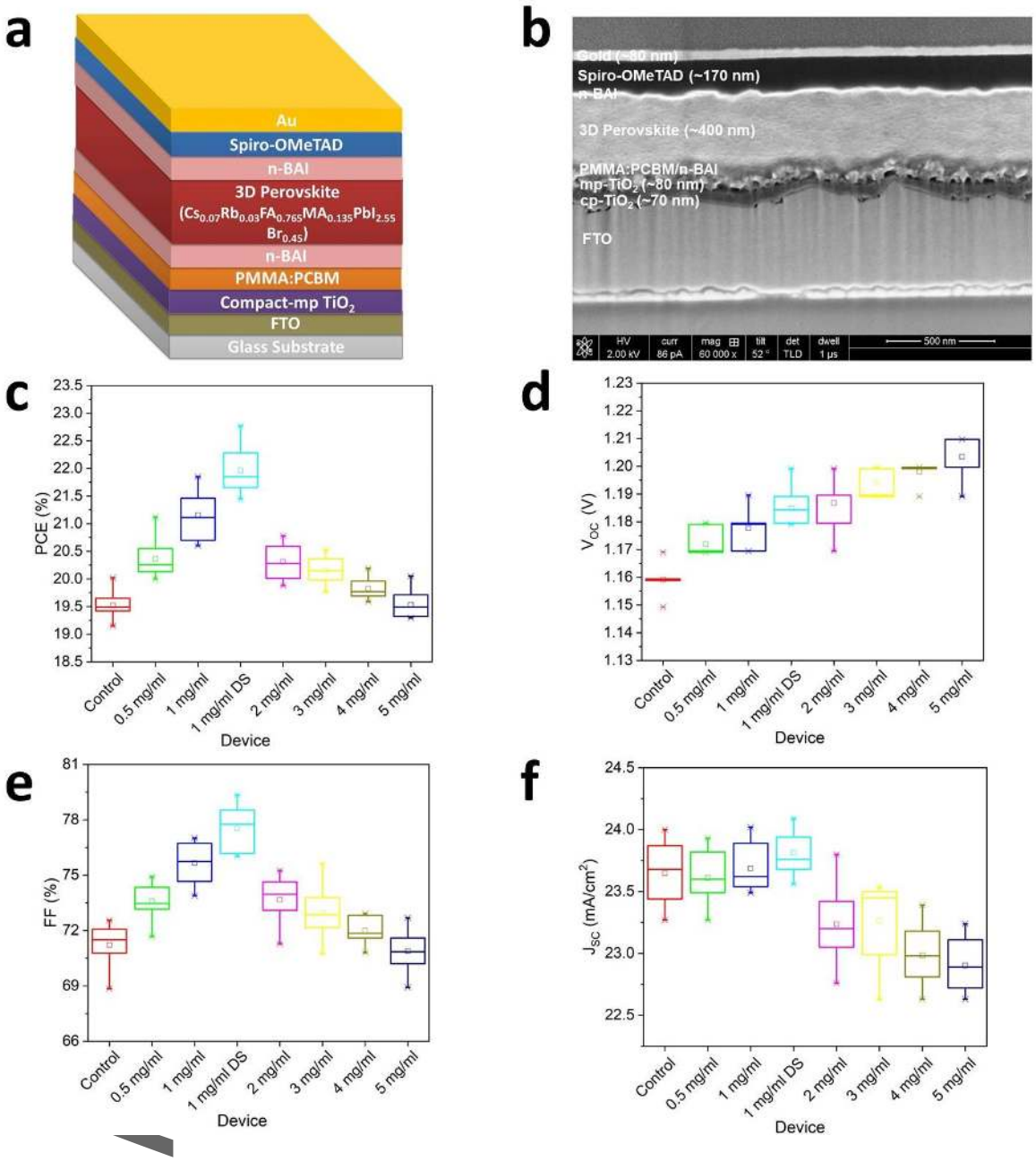

Figure 2. a. Cross-section TEM image of the perovskite device demonstrating the thin 2D perovskite layer at the interface between 3D perovskite and Spiro-OMeTAD HTL, b. Zoom-in view of the highlighted region in Figure 2a, HRTEM image at the interface between 3D and 2D perovskite showing c. the 2D layer thickness and d. the variation in interplanar spacing between the 3D and 2D layer.

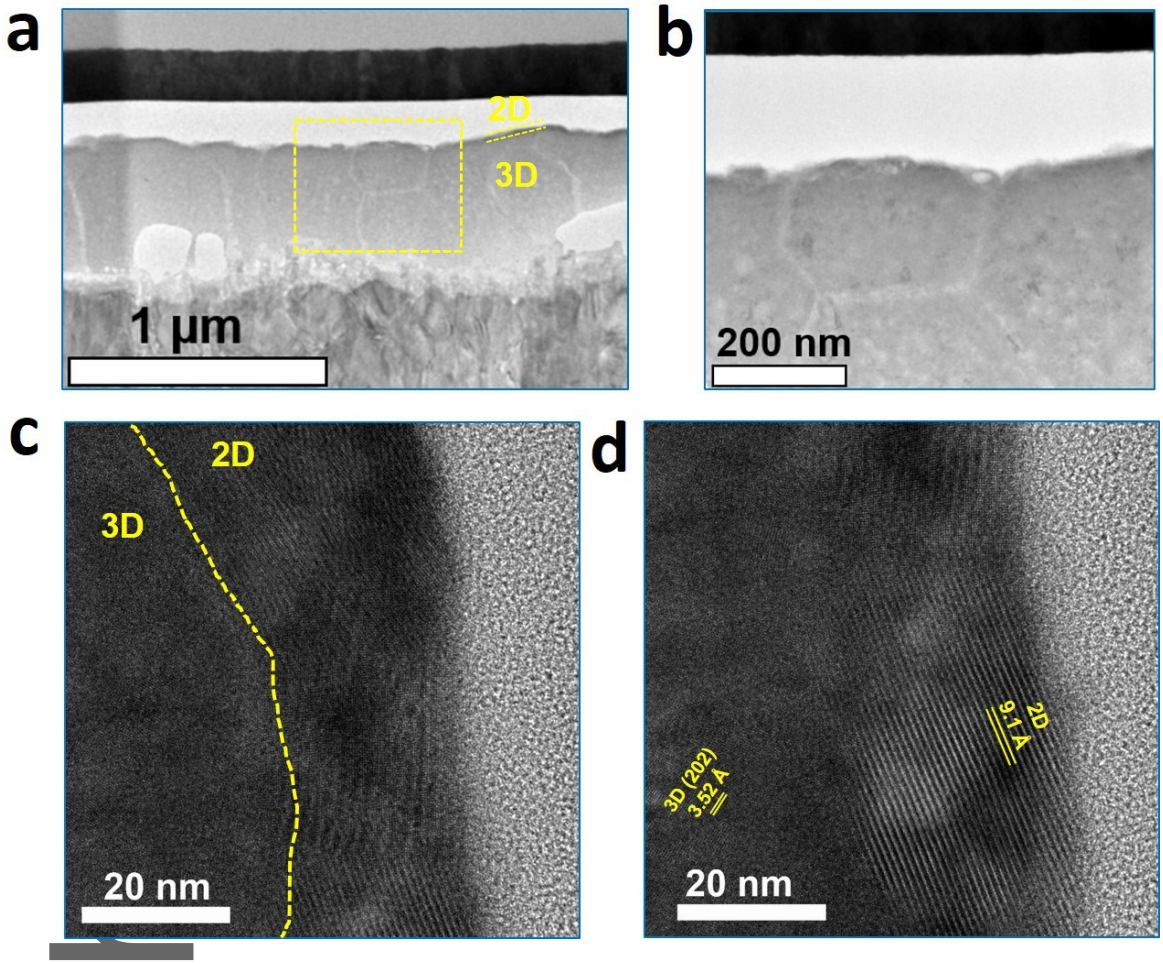

Figure 3. a. Current density-voltage (J-V) curves of the best performing control and double-side passivated PSCs, b. Stabilized efficiency of the respective PSCs at maximum power point (the inset shows the first 40 seconds of the stabilization, demonstrating the variation in transient response of the control and the passivated cells), c. Hysteresis indices of control and double-side passivated PSCs at different scan rates

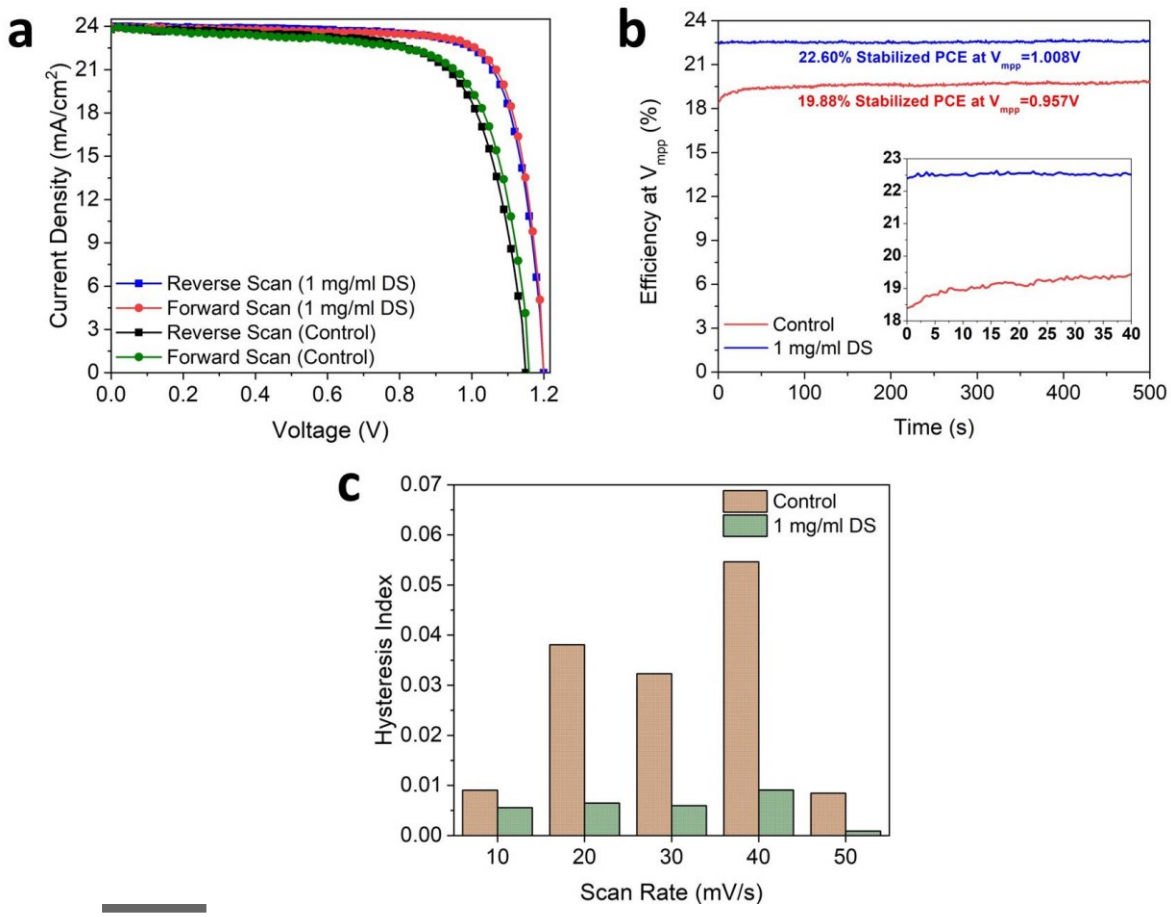

Figure 4. a. Steady-state PL (ST-PL) spectra of control and passivated perovskite films, PL images of b. control, c. 1 mg/ml and d. 1 mg/ml double-side passivated perovskite devices

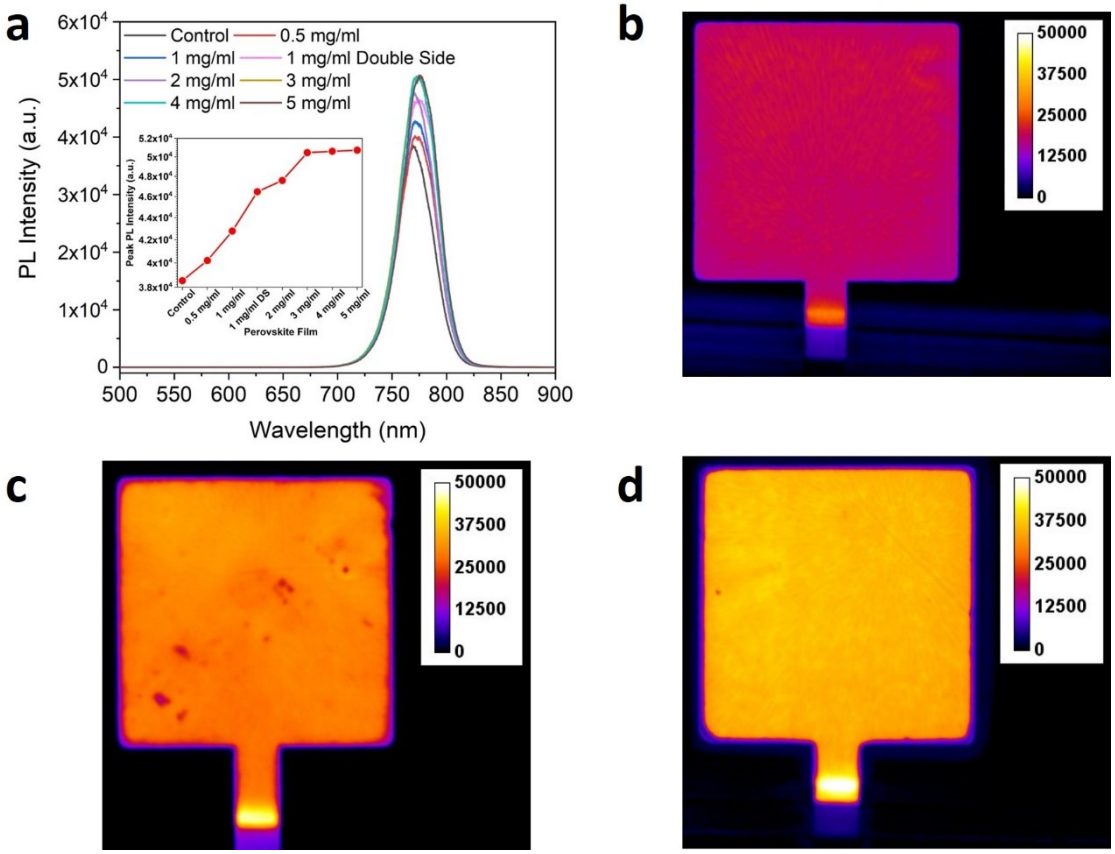

Figure 5. UPS spectra of control, 1 mg/ml, 3 mg/ml and 5 mg/ml perovsite films: a. The secondary electron cut-off region for determining the material workfunction, b. the valence band region and c. The magnified valence band region from UPS spectra and the IPES spectra of the respective films to determine the VBM and CBM of the materials, respectively, d. Energy band diagram illustrating the VBM energy gap between perovskite and TiO_2 ETL and the VBM/HOMO energy gap between perovskite and Spiro-OMeTAD HTL with the incorporation of passivating layers (The UPS measurement allows an error of ±0.1V. The figures are not drawn to the scale)

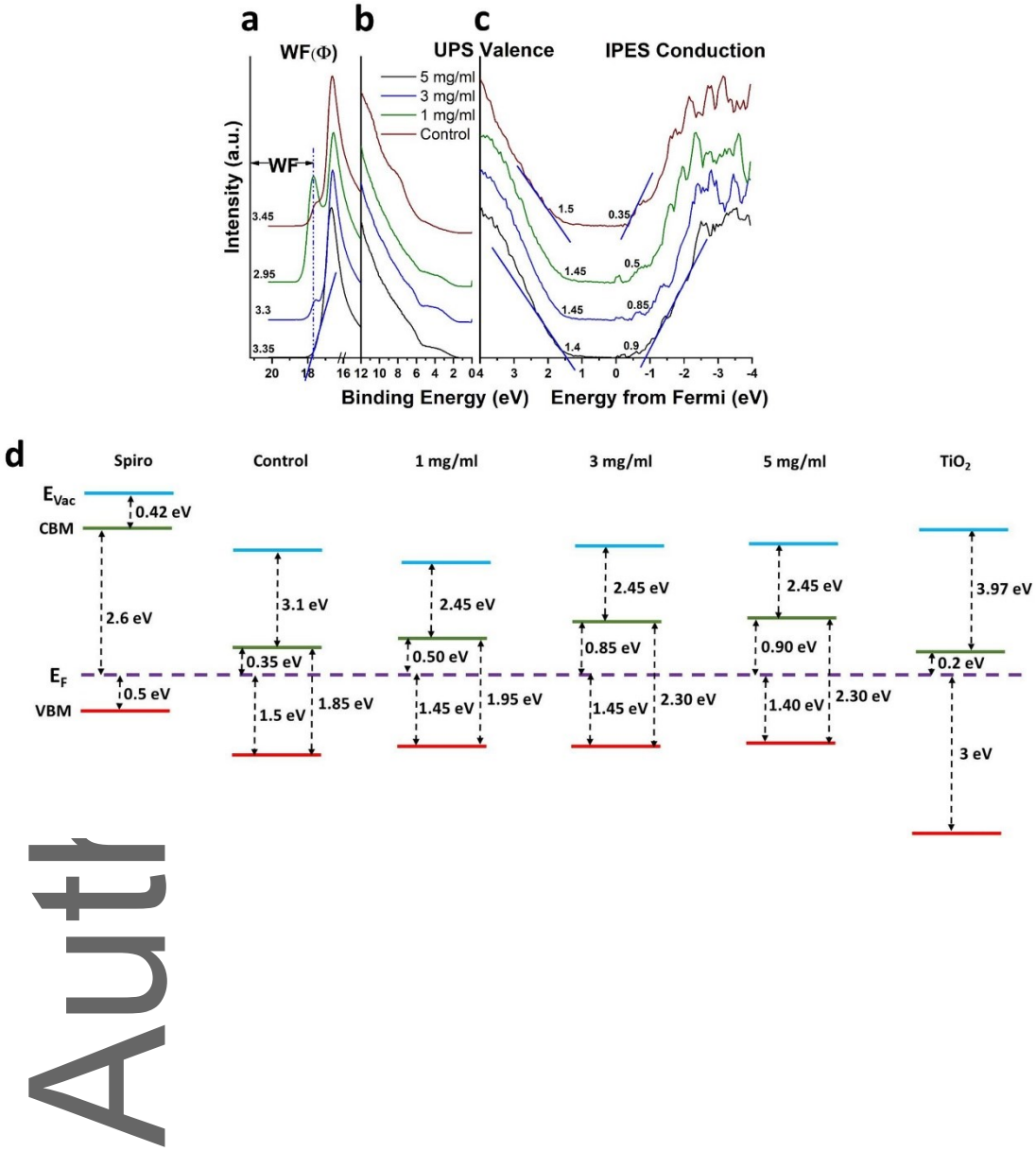

Figure 6. a. Simulated current density-voltage (J-V) curves with voltage sweep rate of 50 mV/s as a function of interface recombination. b. Simulated transient photocurrent at maximum power point (MPP) voltage as a function of interface recombination. The dependence of the short-circuit current density, fill-factor and open-circuit voltage on interface recombination is plotted in figures c.-e., respectively. Both J-V and transient MPP simulations use the same parameter set, detailed in supplementary information.

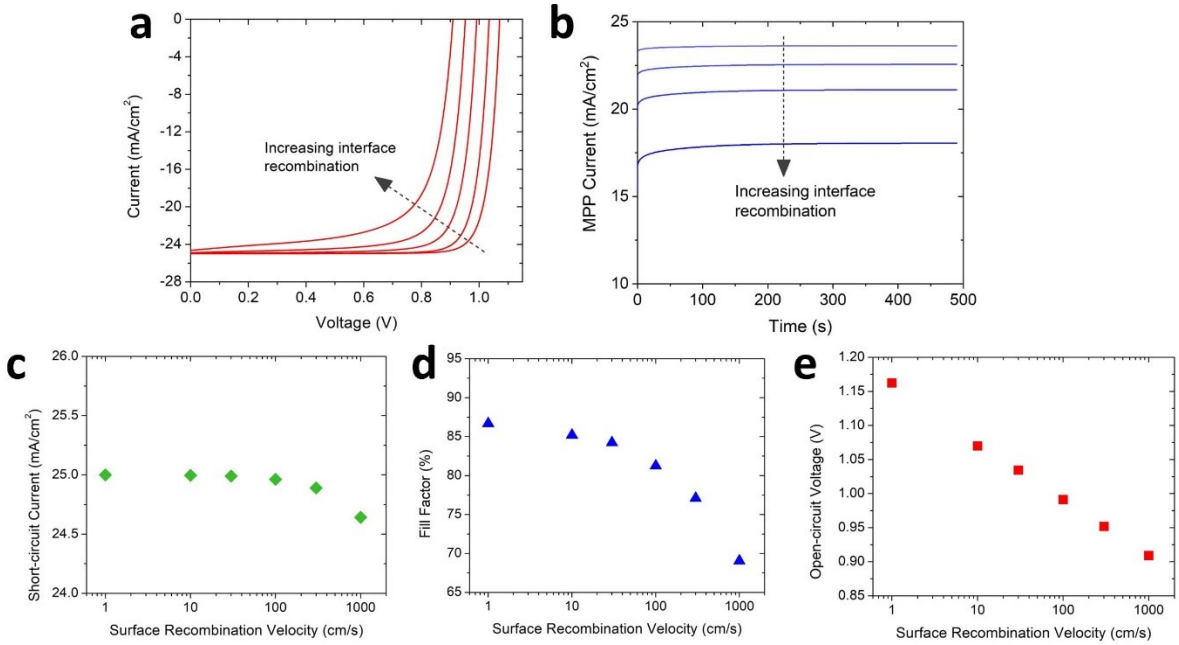

Table of Content Entry

Double-sided 2D surface passivation of 3D perovskite film demonstrates outstanding chemical passivation effect at both interfaces between perovskite and neighboring charge transport layers, contributing to a remarkable V_{OC} of 1.2 V, which is one of the highest open-circuit voltages reported for perovskite cells with an optical bandgap of ~1.6 eV

Keyword Mixed dimensional perovskite solar cells

Double-Sided Surface Passivation of 3D Perovskite Film for High-Efficiency Mixed Dimensional Perovskite Solar Cells

Md Arafat Mahmud[*]*, The Duong, Yanting Yin, Huyen T. Pham, Daniel Walter, Jun Peng, Yiliang Wu, Li Li, Heping Shen, Nandi Wu, Naeimeh Mozaffari, Gunther Andersson, Kylie R. Catchpole, Klaus J. Weber, and Thomas P. White**